Appl. Phys. A (2014) 116:1473–1476
DOI 10.1007/s00339-014-8263-0

Applied Physics A
Materials Science & Processing

Room-temperature ferromagnetism in amorphous In–Ga–Zn–O films fabricated by using pulsed-laser deposition

Shiu-Jen Liu · Shih-Hao Su · Jenh-Yih Juang

Received: 3 December 2013 / Accepted: 15 January 2014 / Published online: 1 February 2014
© Springer-Verlag Berlin Heidelberg 2014

Abstract Room-temperature ferromagnetism (RTFM) was observed in pulsed-laser deposited amorphous In–Ga–Zn–O (a-IGZO) films undoped with impurities containing unpaired *d* or *f* electrons. The presence of oxygen vacancies in the prepared a-IGZO films was verified by X-ray photoelectron spectroscopy and suggested to be responsible for the observed RTFM. The electrical and optical properties of the a-IGZO films were also investigated.

1 Introduction

Diluted magnetic semiconductors (DMS) have attracted interest due to the potential application of both charge and spin of electrons [1–3]. Room-temperature ferromagnetism (RTFM) in DMS is typically realized via doping transition metals (TM) in wide bandgap oxide semiconductors as predicted by theoretical calculation [4, 5]. Actually, a number of studies on TM-doped oxide semiconductors exhibiting RTFM have been reported [6–11]. However, so-called d^0 ferromagnetism is observed in oxide semiconductors doped with elements containing no unpaired *d* or *f* electrons such as N- and C-doped ZnO films [12, 13]. RTFM is also observed in ZnO nano-particles with defects [14], oxygen-deficient SnO_2 [15] and ZnO films [16]. On the other hand, amorphous In–Ga–Zn–O (a-IGZO) with wide bandgap ($E_g = 3.1$–3.5 eV) [17] is a promising material for fabricating optoelectronic devices such as thin-film transistor (TFT). Previous studies demonstrated that the Hall mobility of carriers in a-IGZO films is not significantly affected in amorphous crystal structure even if the films are under bending [18]. It reveals that the electronic structure of a-IGZO is insensitive to chemical bond distortion. The unique feature is believed to be originated from the carrier transport path composed of extended spherical *s* orbitals of heavy metal cations [19] and has attracted much attention on fabricating flexible and transparent TFTs using a-IGZO films as the active channel material. Since a-IGZO has been proven to be suitable for fabricating oxide electronic devices, ferromagnetic a-IGZO would be possible to realize DMS devices. In this paper, we report the RTFM in a-IGZO films undoped with TM. The electrical and optical properties of the a-IGZO films were also investigated.

2 Experiments

The a-IGZO films used in this study were grown on double-side polished *c*-cut sapphires using pulsed-laser deposition (PLD) with a ceramic pellet as the target. The target with a composition ratio of In:Ga:Zn = 2:2:1 at.% was prepared by conventional solid state reactions from a mixture of high-purity (99.95 %) In_2O_3, Ga_2O_3, and ZnO powders. KrF excimer laser ($\lambda \sim 248$ nm) was used to ablate the target with an energy density of 1.5 J/cm^2 per pulse and a repetition rate of 5 Hz. The distance between the target and substrates was 4–5 cm. The growth temperatures (T_s) were kept at room temperature, i.e., 25 °C, (Sample #1) and 150 °C (Sample #2) during PLD. For Sample #2, the film was naturally cooled down to room temperature after PLD. No post-annealing was adopted after the deposition of both

S.-J. Liu (✉)
Department of Mathematics and Science (Pre-college), National Taiwan Normal University, Linkou Dist., New Taipei, Taiwan
e-mail: sjliu@ntnu.edu.tw

S.-H. Su · J.-Y. Juang
Department of Electrophysics, National Chiao Tung University, Hsinchu 300, Taiwan

films. The chamber was evacuated to a base pressure of 10^{-6} torr before the film deposition. The oxygen pressure in the chamber was 10^{-2} torr during PLD. The growth rate is about 0.05 nm/pulse and the thickness of the films is about 130–150 nm. Except the peaks of the sapphire substrates, no signature from the films was observed in X-ray diffraction scans (not shown here), which indicates the amorphous structure of the prepared films. The room-temperature magnetization versus magnetic field $M(H)$ curves were performed on a Quantum Design superconducting quantum interference device magnetometer. The X-ray photoelectron spectroscopy (XPS) analysis was carried out using the Thermo VG Scientific ESCALAB 250 system with a Al Kα X-ray source (1,486.6 eV). The analysis chamber is equipped with a flood gun used for charge compensation when necessary. The XPS spectra are referenced to the C 1*s* photoemission line of 284.8 eV. The Hall effect measurement and van der Pauw method were employed to obtain the electrical properties including resistivity (ρ), carrier density (n) and carrier mobility (μ). The optical transmission and reflection spectra were recorded using an UV–Vis spectrometer.

3 Results and discussion

The field-dependent magnetization $M(H)$ curves measured at room temperature are depicted in Fig. 1. The $M(H)$ curves were taken with fields applied parallel to the plane of films and corrected for the diamagnetism of sapphire substrates. As seen from the $M(H)$ curves, Sample #2 grown at 150 °C evidently exhibits ferromagnetism at room temperature. On the other hand, Sample #1 grown at 25 °C shows a diamagnetic behavior combined with paramagnetism or weak ferromagnetism. The films used in this study were deposited using the same target. And special cares were taken during the sample preparation and measurement procedures to exclude the contribution from magnetic contaminations. The RTFM exhibited by Sample #2 should not be attributed to impurities containing unfilled *d* or *f* shells. The RTFM in oxide compounds undoped with transition metals, i.e., the so-called d^0 ferromagnetism, is generally related to lattice defects such as oxygen vacancies [15, 16], cation interstitials [20] and cation vacancies [21, 22].

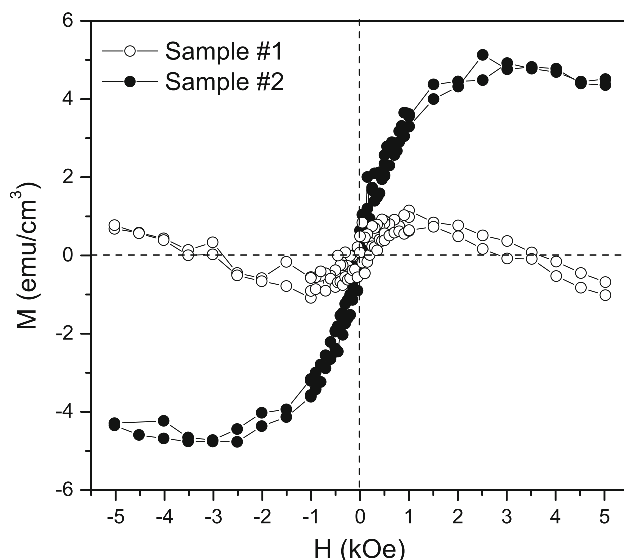

Fig. 1 Room-temperature magnetization (M) as a function of magnetic field (H) of the a-IGZO films. The magnetic fields were applied parallel to the plane of the films

Since oxygen vacancies, cation interstitials and cation vacancies were suggested to play important roles in the RTFM observed in oxide semiconductors, it is necessary to characterize the valence states of cations and oxygen vacancies in the a-IGZO films. Core level In 3*d*, Zn 2*p*, Ga 2*p* and O 1*s* XPS spectra were carried out at room temperature and respectively illustrated in Fig. 2a–d. For In 3*d*, Zn 2*p* and Ga 2*p* XPS spectra shown in Fig. 2a–c, since no obvious difference was observed between the spectra for Sample #1 and #2, the RTFM observed here could not be resulted from the cations. On the other hand, both the O 1*s* XPS curves shown in Fig. 2d can be fitted by combining two symmetric Gaussian peaks. The one with lower binding energy (~530.2 eV) is referred to as the low binding energy component (LBEC) and has been ascribed to the O 1*s* core peak of O^{2-} bound to metal cations [23]. Perhaps, the more relevant peak centered at about 532.1 eV is the high binding energy component (HBEC), which has been suggested to directly relate to the concentration of oxygen vacancies [14, 24]. The HBECs indicate the presence of oxygen vacancy in the a-IGZO films, as revealed by previous studies [17]. Moreover, the areal increment of HBEC in Sample #2 grown at 150 °C indicates the more oxygen vacancies than Sample #1. Therefore, we would like to attribute RTFM observed here to oxygen vacancies which maybe positively charged monovalent (V_O^+) and induce local magnetic moments [25].

Electrical properties ρ, n, and μ of the two samples are listed in Table 1. As shown in the table, the ρ of Sample #2 (4.5×10^{-3} Ω cm) is much lower than that of Sample #1 (0.35 Ω cm) which is mainly resulted from the enhanced μ of Sample #2 by growing at a higher temperature (150 °C) since the carrier densities of these two films are similar, 2.1×10^{19} and 5.9×10^{19} cm^{-3} for Sample #1 and Sample #2, respectively. The high carrier density in a-IGZO films is believed to be induced by oxygen vacancies [17].

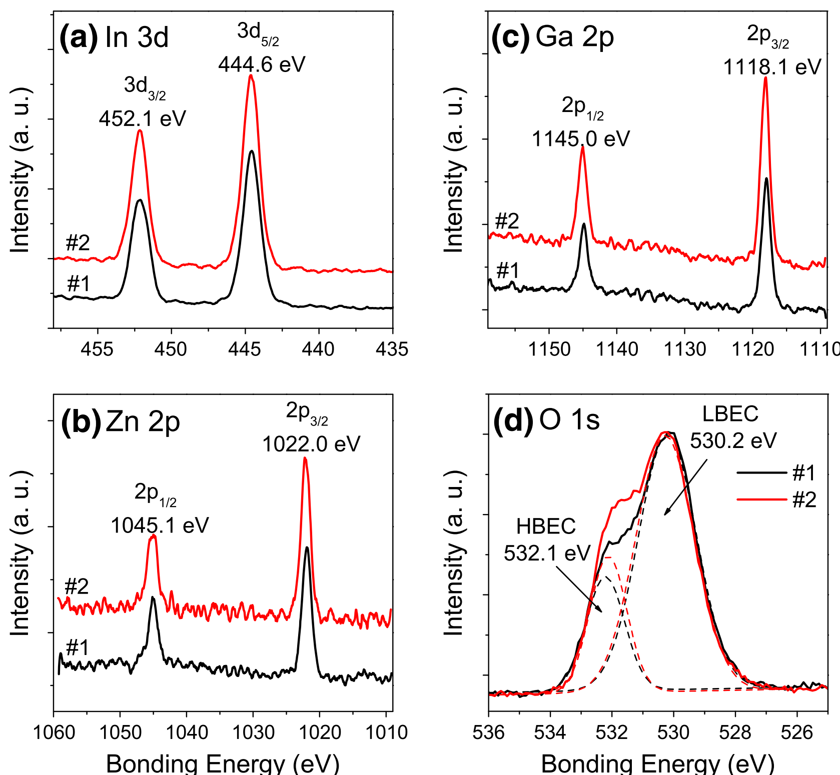

Fig. 2 Core level XPS spectra of **a** In 3*d*, **b** Zn 2*p*, **c** Ga 2*p* and **d** O 1*s* for Sample #1 and Sample #2 grown at 25 and 150 °C, respectively. The *dash lines* plotted in (**d**) are the Gaussian fitting. LBEC and HBEC mean low binding energy component and high binding energy component, respectively

Table 1 Growth temperature (T_s), resistivity (ρ), carrier density (n) and carrier mobility (μ) of the a-IGZO films used in this study

Sample	T_s (°C)	ρ (Ω cm)	n ($\times 10^{19}$ cm^{-3})	μ (cm^2/V s)
#1	25	3.5×10^{-1}	2.1	0.9
#2	150	4.5×10^{-3}	5.9	23.7

Although the XRD results reveal amorphous structures of both films, the low carrier mobility of Sample #1 (< 1 cm^2/V s) indicates that the crystal structure of Sample #1 is more disorder than that of Sample #2 owing to be deposited at a lower temperature, 25 °C. To further explore the transport properties of these two samples, the temperature dependence of electrical resistivity was carried out and is depicted in Fig. 3. Sample #2 shows a degenerate conduction behavior. However, although the carrier density of Sample #1 is as high as 2.1×10^{19} cm^{-3}, the resistivity of Sample #1 increases as the temperature is reduced. Moreover, as shown in the inset of Fig. 3, the resistivity of Sample #1 follows $\rho(T) \sim \exp(T^{-1/4})$ relationship in the temperature range $80 < T < 290$ K. This result is generally explained by the Mott variable-range hopping mechanism describing conduction in strongly disordered systems with localized charge-carrier states [26]. Nevertheless, another possible mechanism suggested by Takagi et. al. [17] for explaining the $\rho(T) \sim \exp(T^{-1/4})$ behavior in amorphous oxide semiconductor is the percolation conduction which has been used to describe the carrier transport in highly doped polycrystalline Si [27].

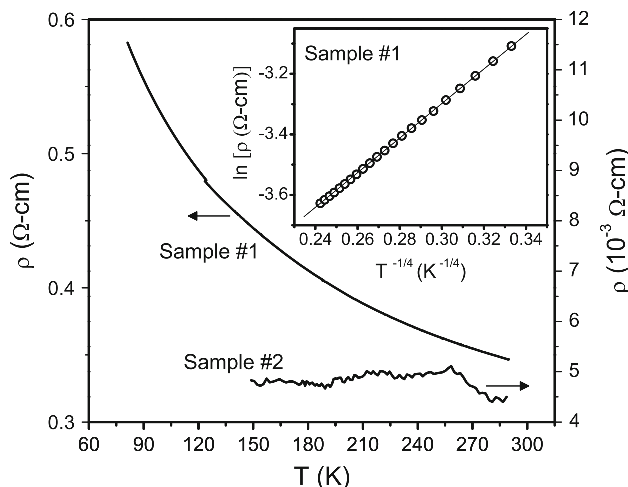

Fig. 3 Temperature dependence of electrical resistivity of Samples #1 and #2. The *inset* shows the ln(ρ) vs $T^{-1/4}$ plot for Sample #1

The optical properties of the prepared a-IGZO films were investigated by measuring the transmission and reflection spectra at room temperature, as illustrated in Fig. 4. First of all, as seen in the figure, the transmission of a-IGZO films is found to be obviously enhanced by raising the film growth temperature to 150 °C. And the average transmission of Sample #2 exceeds 80 % in the visible

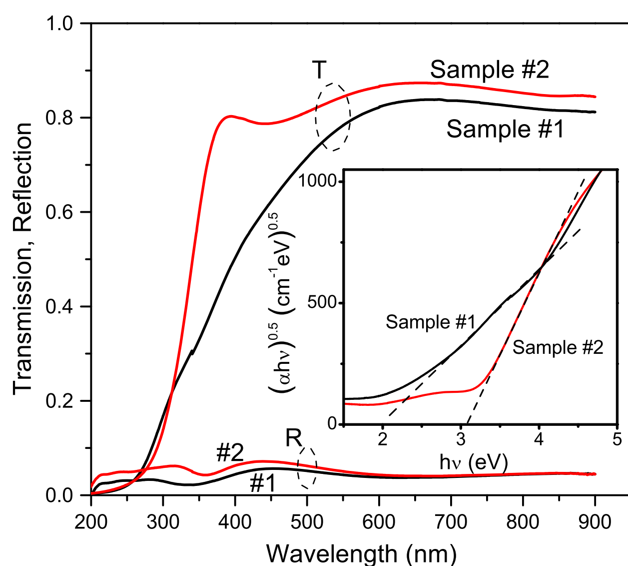

Fig. 4 Optical transmission and reflection spectra of Samples #1 and #2. The *inset* shows the $(\alpha h\nu)^{0.5}$ vs $h\nu$ plots

range (400–700 nm). Furthermore, the optical bandgap (E_g) of transparent conducting oxide films can be estimated by the relationship between absorption coefficient (α) and photon energy ($h\nu$) of the form $(\alpha h\nu) \sim (h\nu - E_g)^r$ with $r = 2$ suggested by Tauc for amorphous semiconductors [28, 29]. The E_g of Sample #2 is then estimated to be 3.1 eV by linear extrapolation of $(\alpha h\nu)^{0.5}$ to the $h\nu$-axis, as depicted in the inset of Fig. 4.

4 Conclusions

In conclusion, electrical, optical and magnetic properties of a-IGZO films grown on sapphires at 25 and 150 °C using pulsed-laser deposition were investigated. RTFM was observed in the a-IGZO film grown at 150 °C, which undoped with impurity containing unpaired *d* or *f* electrons. On the other hand, the a-IGZO film grown at 25 °C exhibits a diamagnetism behavior combined with paramagnetism or weak ferromagnetism. The observed RTFM was attributed to the oxygen vacancies revealed by XPS measurements. The temperature dependance of electrical resistivity of the a-IGZO films grown at 25 °C follows a $\rho(T) \sim \exp(T^{-1/4})$ relationship. The a-IGZO film grown at 150 ° C shows a degenerate conduction behavior. The optical transmission of a-IGZO films can be remarkably enhanced by raising the growth temperature to 150 °C.

Acknowledgments This work was supported by the National Science Council of Taiwan, under Grant Nos. NSC 101-2112-M-003-007.

References

1. S.J. Pearton, C.R. Abernathy, M.E. Overberg, G.T. Thaler, D.P. Norton, N. Theodoropoulou, A.F. Hebard, Y.D. Park, F. Ren, J. Kim, L.A. Boatner, J. Appl. Phys. **93**, 1 (2003)
2. R. Janisch, P. Gopal, N.A. Spaldin, J. Phys.: Condens. Matter **17**, R657 (2005)
3. T. Dietl, J. Phys.: Condens. Matter **19**, 1 (2007)
4. T. Dietl, H. Ohno, F. Matsukura, J. Cibert, D. Ferrand, Science **287**, 1019 (2000)
5. K. Sato, H.K. Yoshida, Jpn. J. Appl. Phys., Part 2 **39**, L555 (2000)
6. Y. Matsumoto, M. Murakami, T. Shono, T. Hasegawa, T. Fukumura, M. Kawasaki, P. Ahmet, T. Chikyow, S. Koshihara, H. Koinuma, Science **291**, 854 (2001)
7. S.B. Ogale, R.J. Choudhary, J.P. Buban, S.E. Lofland, S.R. Shinde, S.N. Kale, V.N. Kulkarni, J. Higgins, C. Lanci, J.R. Simpson, N.D. Browning, S.D. Sarma, H.D. Drew, R.L. Greene, T. Venkatesan, Phys. Rev. Lett. **91**, 077205 (2003)
8. J.M.D. Coey, A.P. Douvalis, C.B. Fitzgerald, M. Venkatesan, Appl. Phys. Lett. **84**, 1332 (2004)
9. K. Ueda, H. Tabata, T. Kawai, Appl. Phys. Lett. **79**, 988 (2001)
10. P. Sharma, A. Gupta, K.V. Rao, F.J. Owens, R. Sharma, R. Ahuja, J.M.O. Guillen, B. Johansson, G.A. Gehring, Nat. Mater. **2**, 673 (2003)
11. S.J. Liu, H.W. Fang, S.H. Su, C.H. Li, J.S. Cherng, J.H. Hsieh, J.Y. Juang, Appl. Phys. Lett. **94**, 092504 (2009)
12. C.F. Yu, T.J. Lin, S.J. Sun, H. Chou, J. Phys. D **40**, 6497 (2007)
13. H. Pan, J.B. Yi, L. Shen, R.Q. Wu, J.H. Yang, J.Y. Lin, Y.P. Feng, J. Ding, L.H. Van, J.H. Yin, Phys. Rev. Lett. **99**, 127201 (2007)
14. X.Y. Xu, C.X. Xu, J. Dai, J.G. Hu, F.J. Li, S. Zhang, J. Phys. Chem. C **116**, 8813 (2012)
15. G.S. Chang, J. Forrest, E.Z. Kurmaev, A.N. Morozovska, M.D. Glinchuk, J.A. McLeod, A. Moewes, T.P. Surkova, N.H. Hong, Phys. Rev. B **85**, 165319 (2012)
16. P. Zhan, W.P. Wang, C. Liu, Y. Hu, Z.C. Li, Z.J. Zhang, P. Zhang, B.Y. Wang, X.Z. Cao, J. Appl. Phys. **111**, 033501 (2012)
17. A. Takagi, K. Nomura, H. Ohta, H. Yanagi, T. Kamiya, M. Hirano, H. Hosono, Thin Solid Films **486**, 38 (2005)
18. K. Nomura, H. Ohta, A. Takagi, M. Hirano, H. Hosono, Nature **432**, 488 (2004)
19. H. Hosono, M. Yasukawa, H. Kawazoe, J. Non-Cryst. Solids **203**, 334 (1996)
20. X. Zhang, Y.H. Cheng, L.Y. Li, H. Liu, X. Zuo, G.H. Wen, L. Li, R.K. Zheng, S.P. Ringer, Phys. Rev. B **80**, 174427 (2009)
21. C.D. Pemmaraju, S. Sanvito, Phys. Rev. Lett. **94**, 217205 (2005)
22. G.Z. Xing, Y.H. Lu, Y.F. Tian, J.B. Yi, C.C. Lim, Y.F. Li, G.P. Li, D.D. Wang, B. Yao, J. Ding, Y.P. Feng, T. Wu, AIP Adv. **1**, 022152 (2011)
23. G. Tyuliev, S. Angelov, Appl. Surf. Sci. **32**, 381 (1988)
24. R.N. Aljawfi, S. Mollah, J. Magn. Magn. Mater. **323**, 3126 (2011)
25. H. Wang, Y. Yan, K. Li, X. Du, Z. Lan, H. Jin, Phys. Stat. Sol. (b) **247**, 444 (2010)
26. N.F. Mott, J. Non-Cryst. Sol. **1**, 1 (1968)
27. D. Adler, L.P. Flora, S.D. Senturia, Solid State Commun. **12**, 9 (1973)
28. J. Tauc (ed.), *Amorphous and Liquid Semiconductors* (Plenum, New York, 1979), pp. 150–220
29. M.K. Jayaraj, K.J. Saji, K. Normura, T. Kamiya, H. Hosono, J. Vac. Sci. Technol. B **26**, 495 (2008)